Post-print version of the paper by Grimsmo et al. in Int J Impact Eng, 85 (2015) 132-145
http://dx.doi.org/10.1016/j.ijimpeng.2015.07.001

An experimental study of static and dynamic behaviour of bolted end-plate joints of steel

E. L. Grimsmo*, A. H. Clausen, M. Langseth, A. Aalberg

Structural Impact Laboratory (SIMLab), Centre for Research-based Innovation and Department of Structural Engineering, Norwegian University of Science and Technology, NO-7491 Trondheim, Norway
*Corresponding author. Email address: erik.l.grimsmo@ntnu.no.

Abstract

Many actions, such as accidental or malicious explosions, may impose high loading rates to structural frames. To enhance the knowledge of the behaviour of joints subjected to severe impulsive loading, a double-sided beam-to-column joint configuration was tested at quasi-static and dynamic loading rates. The test specimens consisted of H-section beams and columns, extended end-plates, and high-strength bolts. In both the quasi-static and dynamic tests, the fracture modes were bolt failure in combination with plastic deformation of the end-plates. However, it was observed that the joints absorbed considerably more energy before failure in the dynamic tests than in the quasi-static tests, partly due to changes in the deformation modes. Also, the ductility of the joints seemed to increase for higher loading rates. These results suggest that the tested joints behave in a preferable manner under extreme impulsive loads.

Keywords: quasi-static; dynamic; impact; experiments; joints; connections

1 Introduction

The behaviour of steel joints under static loading conditions has been studied extensively in the open literature, and several design codes provide guidelines for calculation of the resistance. On the other hand, the behaviour of steel joints subjected to severe impulsive loading is less documented. In the past decade, after the attack on the World Trade Center in New York in 2001, there has been increased interest in the behaviour of steel structures under extreme loading conditions [1-5]. The design code Unified Facilities Criteria [6] states that joints subjected to blast loads should have adequate strength, stiffness, and rotation capacity. Even though a joint has

satisfactory properties for static load conditions, it does not necessarily behave in a favourable manner under impulsive load conditions. It is therefore important to acquire knowledge about the behaviour of joints subjected to severe dynamic loading.

Several publications present experimental studies on the scenario where the loss of a column in a framed structure cause an abnormal load situation for the adjacent joints, e.g. [2, 5, 7, 8]. In most of these mentioned studies, the load is applied quasi-statically. The exception is the paper by Liu et al. [2], which presents experiments where a test specimen consisting of two beams joined with a central column was subjected to a sudden vertical movement. The reported failure mode was fracture in the web angles, and it was similar in both the dynamic and quasi-static tests.

Sabuwala et al. [3] and Tyas et al. [4] express that there is lack of experimental data published on the behaviour of steel connections subjected to extreme, non-cyclical loading. Karns et al. [9] report the results from tests where double-sided beam-to-column joint configurations were subjected to an explosion blast and subsequent progressive collapse load conditions. Joints with various connections were tested and it was found that the joints can behave in a very ductile manner, even when subjected to high strain-rates. Recently a research group in England started an extensive test program of dynamic tests on bolted steel joints, where single-sided beam-to-column joints loaded at very high strain rates are studied [4, 10, 11]. They report that dynamic effects increased the stiffness and decreased the ductility of joints with the flexible end-plate connections [4].

The test specimens in the current study represent a typical joint configuration within a framed steel structure; two short beams were connected to a short column by end-plate connections. A test series comprising of four quasi-static tests was performed, where the test specimens were gradually loaded until failure by a hydraulic actuator. Further, eight dynamic tests were carried out in a test rig designed for impact testing, where the impact velocity was varied. The purpose of the experimental programme was to study and compare the quasi-static and dynamic response of the joints. More specifically, the deformation modes, evolution of force-displacement response, and energy absorption have been studied. The test set-up and boundary conditions were designed to provide mainly moment and shear in the joints, and the effect of axial forces in the beams was thus not considered. Moreover, the tests were performed with the intention of producing results that can validate numerical models in future studies, and a simple test arrangement was therefore chosen. The test results demonstrate that the behaviour under quasi-static and dynamic load conditions were similar in some aspects. For instance, failure of the joints occurred by tensile bolt fracture for

both load conditions. However, the dynamic tests produced different deformation modes, which induced for example more shear deformation of the bolts. Furthermore, the energy absorption and ductility of the joints seemed to increase in the dynamic tests compared with the quasi-static tests.

2 Experimental programme

2.1 Test specimens

Figure 1a and b display the two types of test specimens studied in the experimental programme. The beams and column of the test specimens were short lengths of rolled steel sections of type HEA 180 and HEB 220, respectively. The weight of the beam lengths was 34.5 ± 0.3 kg each, while the column was 60.3 ± 0.3 kg. End-plates with 12 mm thickness were welded to the beams with a continuous fillet weld with a throat thickness of 5 mm. Figure 1c depicts the cross-section of the beam and the dimensions of the end-plate. All sections and end-plates were of steel grade S355. Six partially threaded M16 bolts of grade 8.8 were used to connect each end-plate to the respective column flange.

Figure 1a and b also indicate the loading and boundary conditions of the specimens. A force was applied to the column, while the end of the beams was fixed in the direction of the force. The load configuration in Figure 1a induces two rows of bolts in tension, and is referred to as the *Design Load Direction* (DLD), because the joints at hand are in practical applications loaded in this direction. Stiffener plates of 10 mm thickness were welded to the column in the compression region, parallel to the beam flanges. This was done to avoid potential buckling of the column web, which would inhibit a controlled deformation to failure. The specimen in Figure 1b is identical to the specimen in Figure 1a, except that it is rotated 180 degrees in the plane and the stiffeners are here moved parallel to the opposite beam flanges. This provides a load configuration where only

Post-print version of the paper by Grimsmo et al. in Int J Impact Eng, 85 (2015) 132-145
http://dx.doi.org/10.1016/j.ijimpeng.2015.07.001

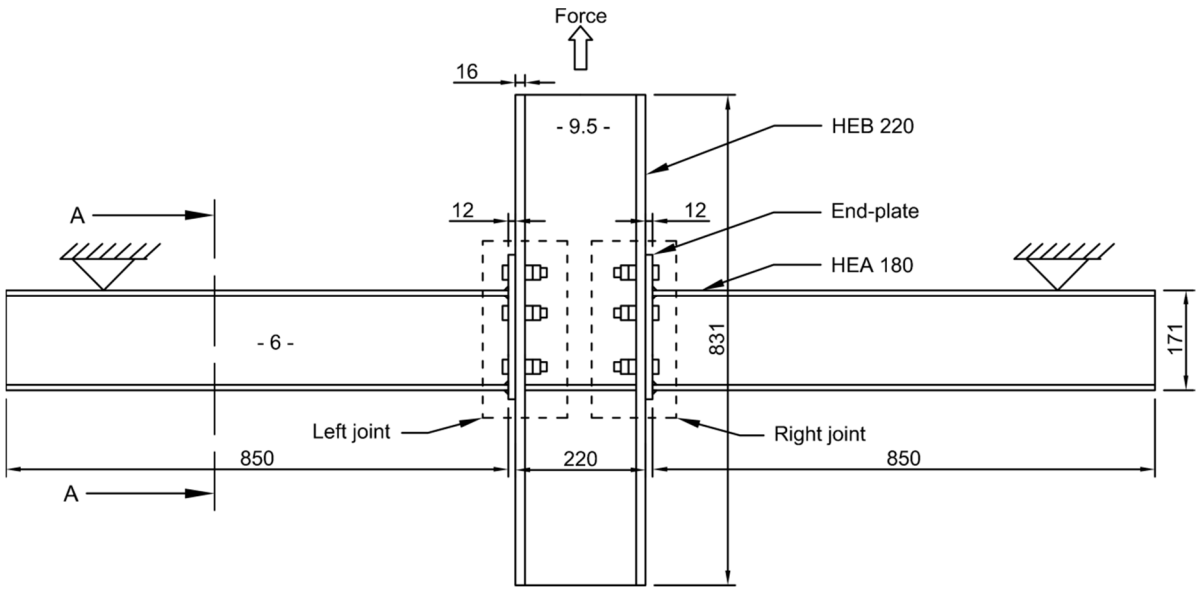

a) Elevation view of the Design Load Direction (DLD) specimen

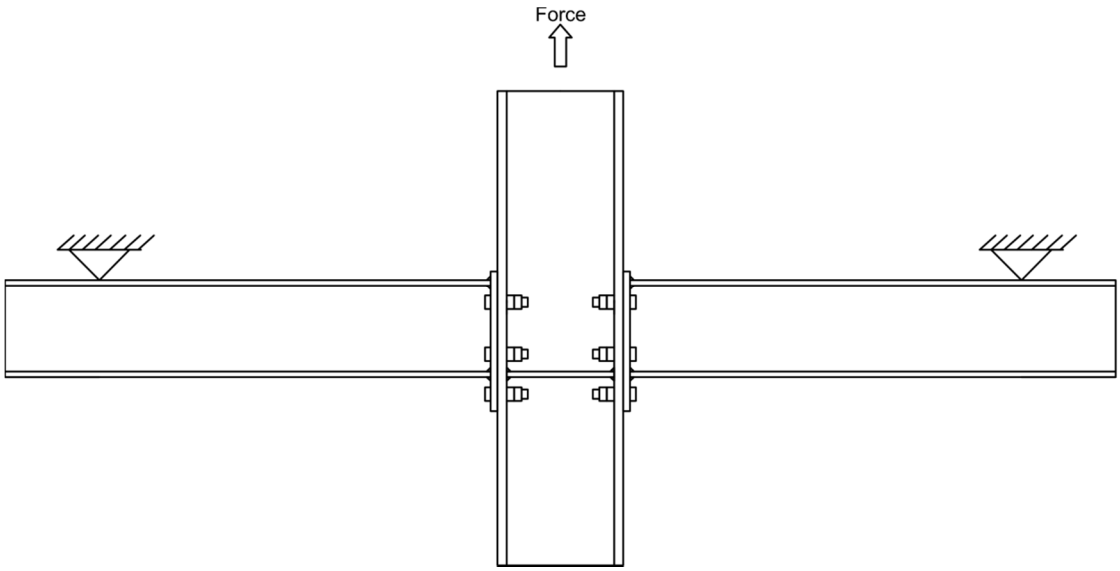

b) Elevation view of the Reverse Load Direction (RLD) specimen, which is similar to the specimen in a), just rotated 180 degrees in the plane and the stiffeners at the web of the column is moved.

Post-print version of the paper by Grimsmo et al. in Int J Impact Eng, 85 (2015) 132-145
http://dx.doi.org/10.1016/j.ijimpeng.2015.07.001

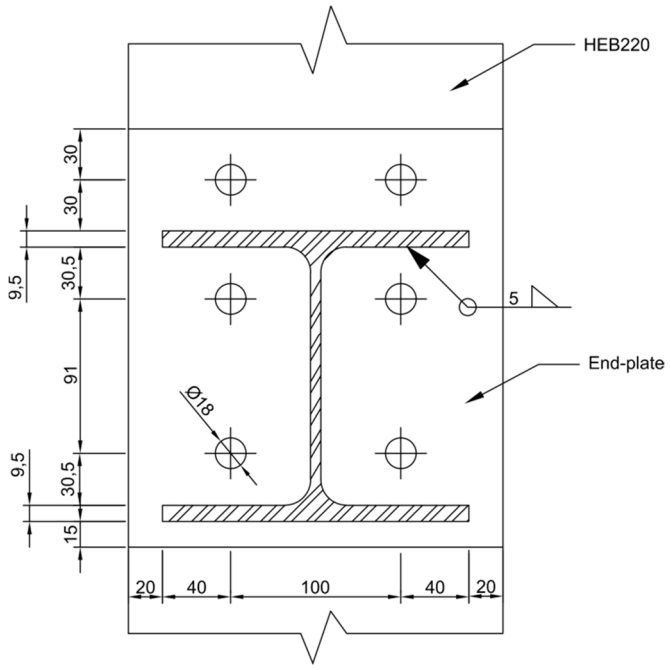

c) Section (A-A) view of the end-plate and cross-section of the beam for DLD specimen

Figure 1 - Dimensions, loading, and boundary conditions of the two types of test specimens.

one bolt row is in tension. The latter load case is denoted the *Reverse Load Direction* (RLD), and is related to for instance the load conditions in a column-loss scenario. For later reference, the specimens in Figure 1a and b have a double-sided joint configuration that consists of left and right joints (indicated in Figure 1a). This terminology is similar to the definitions in Figure 1.1 in NS-EN 1993-1-8, Eurocode 3: Design of steel structures - Part 1-8: Design of joints [12] (hereafter denoted Eurocode 3).

Firm contact between the end-plates and column flanges was achieved by applying a tightening moment of 80 Nm to the bolt and nut assemblies. Two nuts were used on each bolt to prevent thread failure. The reason for this choice is discussed in Section 3.1. Washers were not used.

The dimensions of the test specimens were chosen with regard to the available space in the dynamic test rig. Details of this test rig are presented in Section 2.4. Another deciding factor for the dimensions of the test specimens was that ductile fracture of the joints was preferred. Ductile fracture means that relatively large plastic deformations would appear before ultimate failure in the

test specimen. The joints were therefore designed such that the failure mode that gave the lowest resistance was tensile bolt fracture, partially due to prying effects induced by local bending deformation of the end-plate, according to the calculation procedure in Eurocode 3 [12].

2.2 Mechanical properties

The test specimens described in the previous section were made of profiles, end-plates and bolts coming from the same production batch, respectively. A material test series consisting of quasi-static and dynamic uniaxial tension tests was performed to determine relevant mechanical properties of the materials.

Figure 2 displays representative engineering stress-strain curves acquired from the different materials, where the strain rate was approximately 10^{-4} s^{-1}, which is in the order of magnitude of the strain rate expected in the quasi-static component tests. The curves show data up to the onset of diffuse necking. All the tests in Figure 2 were repeated twice and an excellent agreement between the replicate tests was achieved.

It is reasonable to assume that the strain-rate sensitivity is approximately the same for the S355 steel in the profiles and end-plates. Thus, a strain-rate sensitivity investigation performed only on the end-plate and bolt material was assumed sufficient. Tests at low and medium speeds were

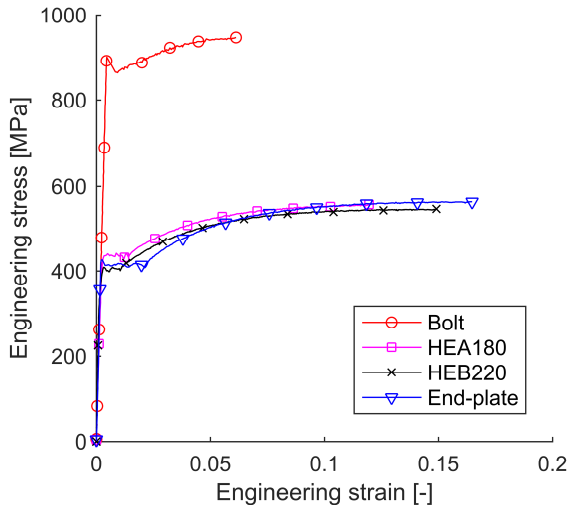

Figure 2 - Engineering stress-strain curves obtained from representative quasi-static uniaxial tension tests.

Post-print version of the paper by Grimsmo et al. in Int J Impact Eng, 85 (2015) 132-145
http://dx.doi.org/10.1016/j.ijimpeng.2015.07.001

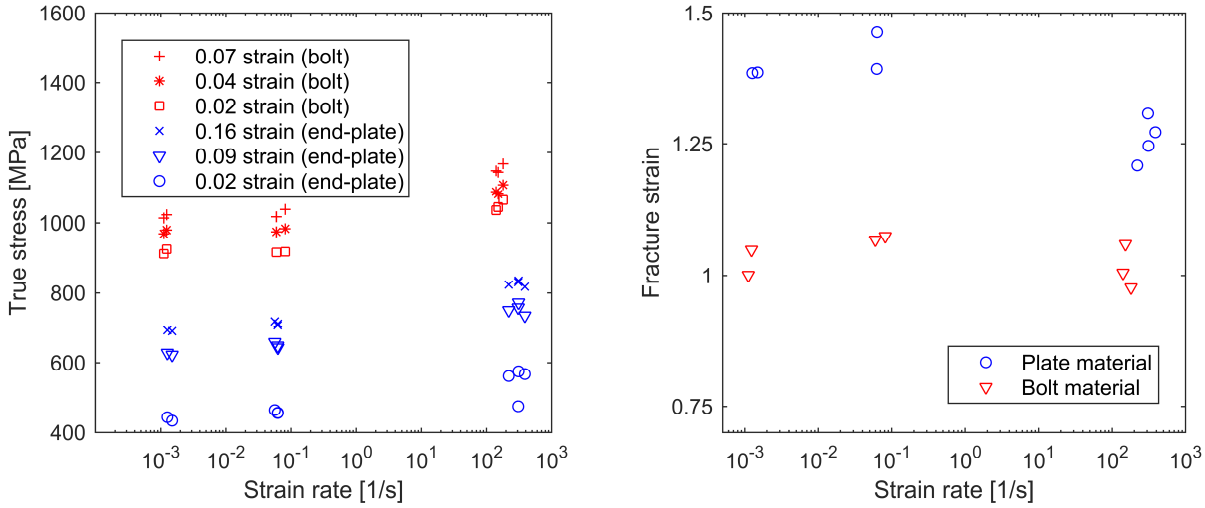

a) True stress at certain strain levels

b) Logarithmic fracture strain

Figure 3 - Strain-rate sensitivity of the stress and fracture strain for the end-plate and bolt material

carried out using a standard servo hydraulic test machine, while high-speed tests were executed with a split-Hopkinson tension bar, applying the methods described by Vilamosa et al. [13]. Figure 3a provides the obtained true stress at certain values of strain as a function of strain rate. Both the end-plate and bolt material exhibited strain-rate dependence with respect to the stress.

The fracture strain of the end-plate and bolt material was determined from optical measurements of the fracture surface area of the ruptured tensile specimens used in the strain-rate sensitivity investigation. By the assumption of conservation of volume during plastic deformation, the logarithmic fracture strain was calculated as $\varepsilon = \ln(A_0/A_f)$, where A_0 and A_f are respectively the areas of the initial cross-section and fracture surfaces of the specimen. Figure 3b displays the acquired fracture strain versus strain rate. The fracture strain of the plate material is slightly reduced at the highest strain rate, whereas no clear dependency is obtained for the bolt material. Dey et al. [14] also observed that steels with a low strength tended to lose ductility as the strain rate increased, while steels with a high strength exhibited no noticeable effect. As all measured fracture strains in the strain rate investigation were around 1 or larger, both materials may be considered ductile at the range of strain rates covered in the component tests.

Post-print version of the paper by Grimsmo et al. in Int J Impact Eng, 85 (2015) 132-145
http://dx.doi.org/10.1016/j.ijimpeng.2015.07.001

2.3 Set-up for quasi-static component tests

The test set-up for the quasi-static tests of the joint configuration is displayed in Figure 4a. A bolted grip connection at the upper end of the column of the test specimen transferred the vertical force P to the test specimen. The force was recorded by a load cell connected in series with a hydraulic actuator (not shown in Figure 4a). A hinge between the load cell and test specimen ensured that no bending moments were transferred to the load cell. One portal frame at each side served as supports for the beams, and thus restricted vertical displacement of the tip of the beams as the actuator pulled the column. Pulling the test specimen upwards rather than pushing it downwards was done because the former choice is geometrically more stable.

As can be observed from Figure 4b, the distance from the support points to the end-plates was 685 mm at each side of the column. The specimens were instrumented with three linear variable displacement transducers (LVDTs), also displayed in Figure 4b. The left and right LVDT, denoted $LVDT_L$ and $LVDT_R$, measured any vertical displacement of the supports, while the centrally located $LVDT_C$ recorded the vertical displacement of the bottom end of the column. This allowed for determination of the vertical displacement of the column relative to the supports. Two cameras dedicated for digital image correlation (DIC) analysis were set up to enable determination of the deformations of the end-plates and column flanges throughout the test.

Four quasi-static tests were performed in total. Two of the test specimens were loaded in the DLD direction and two in the RLD direction, see Figure 1. The quasi-static tests were carried out under displacement control with a constant displacement rate of 0.05 mm/s until failure, which occurred

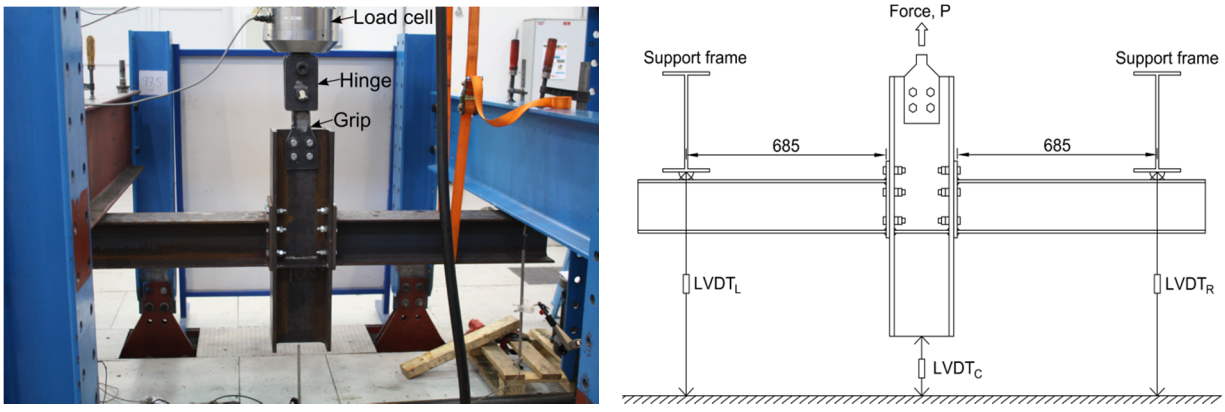

a) Photo of quasi-static test set-up b) Location of supports and LVDTs

Figure 4 - Quasi-static component test set-up.

Post-print version of the paper by Grimsmo et al. in Int J Impact Eng, 85 (2015) 132-145
http://dx.doi.org/10.1016/j.ijimpeng.2015.07.001

by fracture of one or more bolts. The sampling frequency of the load cell, strain gauges, and LVDTs was 2 Hz, while the frame frequency of the cameras was 1 Hz.

By applying the resistance formulas in Eurocode 3 and the distance from the column flange to the support points, the maximum static force P that can be applied to the column is 202 and 87 kN for the DLD and RLD configuration, respectively. In the calculations, measured material properties were used as input and the partial factors γ_{M0} and γ_{M2} were set to unity. The shear force resistance of six bolts in pure shear is 685 kN, according to Eurocode 3.

2.4 Set-up for dynamic component tests

The dynamic component tests were carried out with a pendulum accelerator, which is a test rig made for impact testing of structural components, see Figure 5. Details of this test rig are provided by Hanssen et al. [15]. Therefore, only the main aspects of the rig are given here. As shown in Figure 5, a hydraulic/pneumatic actuator pushes a rotating arm around a set of bearings. The end of the arm is in contact with a trolley on rails such that the trolley is accelerated as the arm rotates. The weight of the trolley was 726.7 kg. The contact between the arm and the trolley is lost after a certain amount of rotation, and subsequently, the trolley travels along the rails with an approximately constant velocity towards the test specimen, which is supported at the reaction wall. Figure 6 provides more details on how the test specimen was oriented at the reaction wall. The two beams were mounted vertically, and the trolley hit the column. A thick plate (here called impact plate) was welded to the end of the column to ensure that the impact force was transferred to the entire section, and thus limited the local plastic deformation at the point of impact.

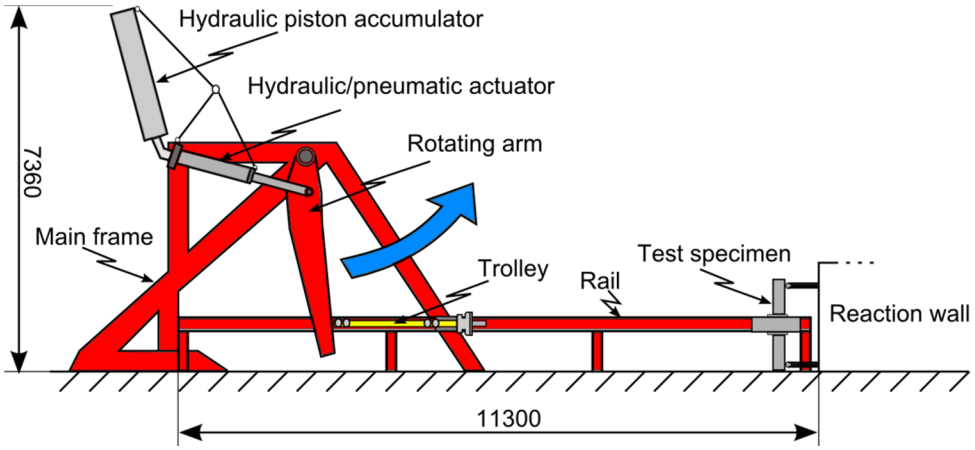

Figure 5 - Schematic illustration of the pendulum accelerator applied in dynamic tests. The part of the main frame and the rail closest to the view point are left out for clarity.

Post-print version of the paper by Grimsmo et al. in Int J Impact Eng, 85 (2015) 132-145
http://dx.doi.org/10.1016/j.ijimpeng.2015.07.001

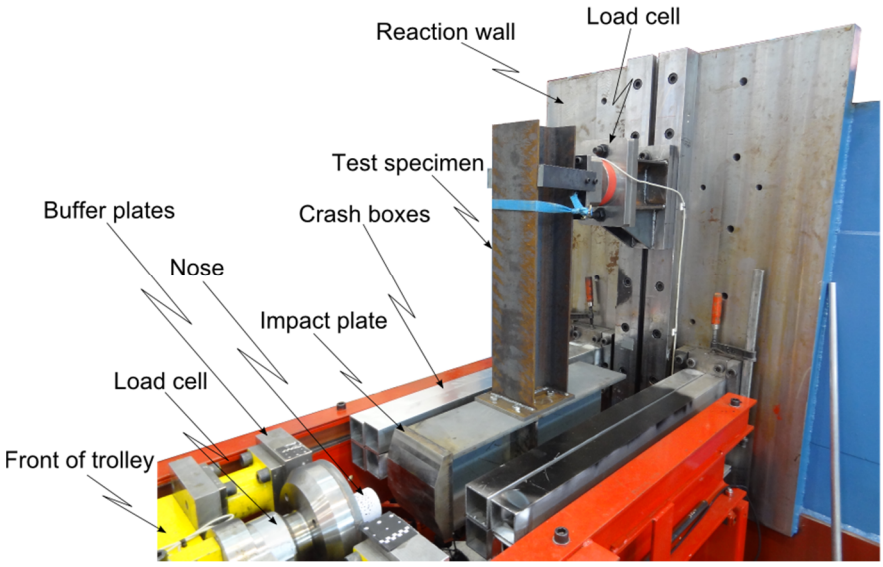

Figure 6 - Detailed view of attachment of the test specimen to the dynamic test rig.

During testing, the nose of the trolley hits the impact plate first, which then causes the column of the test specimen to accelerate towards the reaction wall, which further loads the joints. After 80 to 100 mm displacement of the trolley, the rigid buffer plates of the trolley hit the aluminium crash boxes, and the trolley is then rapidly decelerated. As indicated in Figure 6, a load cell was placed at the front of the trolley, and another at the supported end of the upper beam. A more detailed overview of the instrumentation and supports of the test specimen is provided in Figure 7. For more details on the trolley and the load cell located at the front of the trolley, see the appendix.

A photo cell system, which was located on top of one of the rails, measured the velocity of the trolley immediately before impact and also triggered the data logging system. As illustrated in Figure 7, a laser device with a fixed position relative to the rails was used to measure the displacement of the trolley and any possible displacements of the reaction wall. Moreover, although not shown in Figure 7, two high-speed cameras captured the upper part of the test specimen. One camera focused only on the joint region, providing information on the local deformation of the end-plate and column flange, while the other camera captured the upper half of the test specimen. The frame frequency of the cameras was 16 000 Hz, while the acquisition frequency of the two load cells and the laser was 250 000 Hz.

Post-print version of the paper by Grimsmo et al. in Int J Impact Eng, 85 (2015) 132-145
http://dx.doi.org/10.1016/j.ijimpeng.2015.07.001

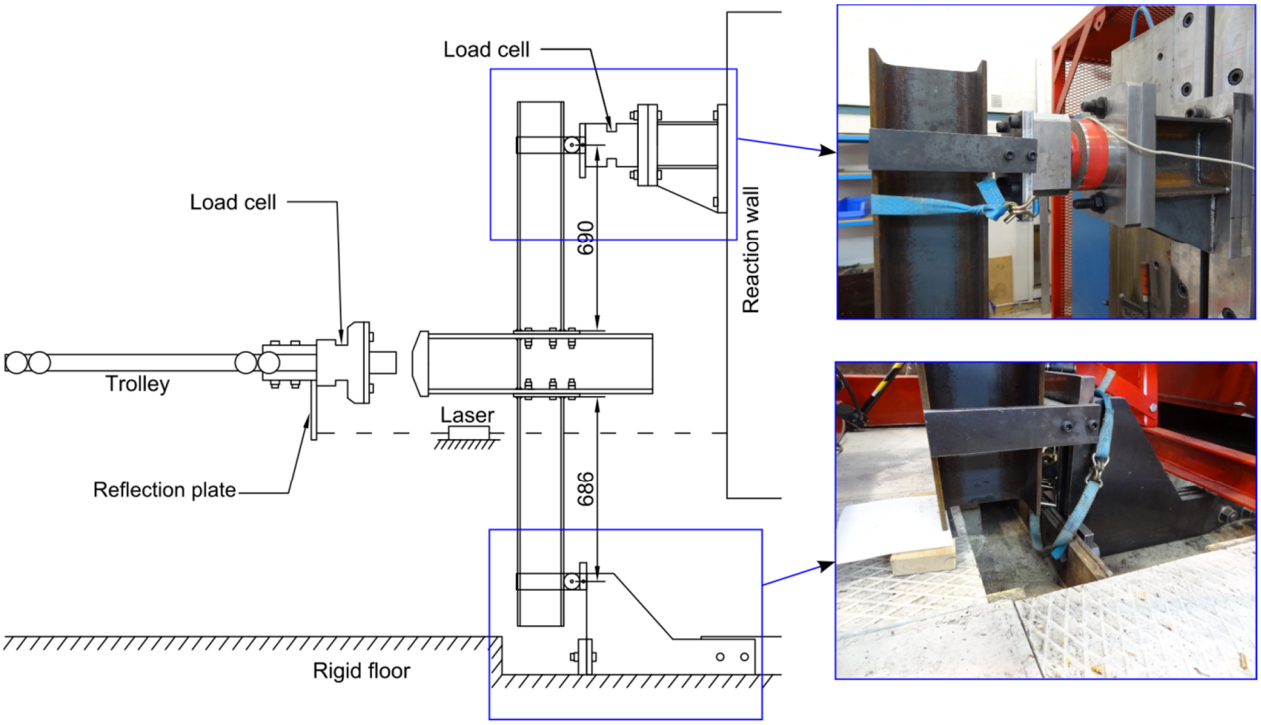

Figure 7 - Instrumentation and fixture of the test specimen in the dynamic tests. For clarity, less important details of the set-up are omitted.

The reaction wall rested on neoprene supports and weighed approximately 150 000 kg. Only the upper support in Figure 7 was connected to the reaction wall, while the lower support was fixed to the laboratory floor by means of thick steel plates. The distances from the end-plates of the joint to the support points were nearly the same as shown for the quasi-static test set-up in Figure 4b. In the dynamic tests there was, however, a small difference between the distance to the upper and lower supports, see Figure 7. The reason for this was that during the testing it was experienced that perfect symmetry until failure was hard to achieve as fracture in the bolts inevitably occurred at one joint before the other. It was more convenient to capture the deformation of the upper end-plate in Figure 7 with a high-speed camera. A 4 mm longer distance to the top support was therefore introduced such that fracture in the upper end-plate and bolts was slightly more likely to happen first.

The entire test program is summarized in Table 1, where the tests are numbered in the order they were performed. The label QS abbreviate quasi-static, and as mentioned in the previous section, two tests of each configuration, DLD and RLD, were performed with a displacement rate of 0.05 mm/s. A total of eight dynamic tests were carried out, tests 5 through 12. Four of these tests were performed at what will be referred to as low speed (LS). More specifically, two of these four tests

were carried out on the RLD configuration and the impact velocity of the trolley was approximately 6 m/s. The velocity in the two tests of the DLD configuration was close to 8 m/s. Finally, the last four tests were all carried out with a velocity of nearly 12 m/s, and these tests will be referred to as high-speed (HS) tests. Two tests each of DLD and RLD configurations were carried out with high speed.

Table 1 - The test names and their corresponding speed.

Test name	Speed [m/s]
QS-RLD-1	$5{\cdot}10^{-5}$
QS-DLD-2	$5{\cdot}10^{-5}$
QS-RLD-3	$5{\cdot}10^{-5}$
QS-DLD-4	$5{\cdot}10^{-5}$
LS-RLD-5	6.02
LS-DLD-6	7.89
LS-DLD-7	7.87
LS-RLD-8	6.00
HS-RLD-9	11.89
HS-DLD-10	11.87
HS-DLD-11	11.83
HS-RLD-12	11.85

3 Results

3.1 Quasi-static component tests

Figure 8 presents photos of the deformed specimens from two tests, one of each load case DLD and RLD, at four stages during the tests. The first picture frames are from the beginning of the tests, while the last frames were taken immediately after bolt fracture. In addition, the corresponding force P and displacement D are specified beneath each photo. The force P was determined with the load cell mounted in series with the hydraulic actuator, see Figure 4a. The displacement D is the relative displacement of the column with respect to the supports. It was calculated from $D = D_C - (D_R + D_L)/2$, where D_C, D_R, and D_L are the displacements measured by $\mathrm{LVDT_C}$, $\mathrm{LVDT_R}$, and $\mathrm{LVDT_L}$, respectively, see Figure 4b. In this equation, the term $(D_R + D_L)/2$ is the average vertical displacement at the supports and represents the rigid-body displacements experienced by the entire specimen due to the inevitable flexibility of the support frames. Validation of the displacement measurements was achieved by comparing the

Post-print version of the paper by Grimsmo et al. in Int J Impact Eng, 85 (2015) 132-145
http://dx.doi.org/10.1016/j.ijimpeng.2015.07.001

displacement acquired from transducer $LVDT_C$ and DIC analysis, and an excellent agreement was found.

As predicted by Eurocode 3 calculations of resistance, the failure mode with the lowest resistance was a combination of end-plate yield-mechanisms and bolt fracture for both load directions, DLD and RLD. The four bolts in tension at the right joint fractured practically simultaneously for the DLD test, while two bolts failed in tension for the RLD test, see the picture frames to the far right in Figure 8. Due to small imperfections in the test specimen or set-up, the deformation mode of the test specimen became inevitably asymmetrical after reaching maximum applied force. This eventually led to bolt failure in one of the joints, i.e. at one of the sides of the joint configuration.

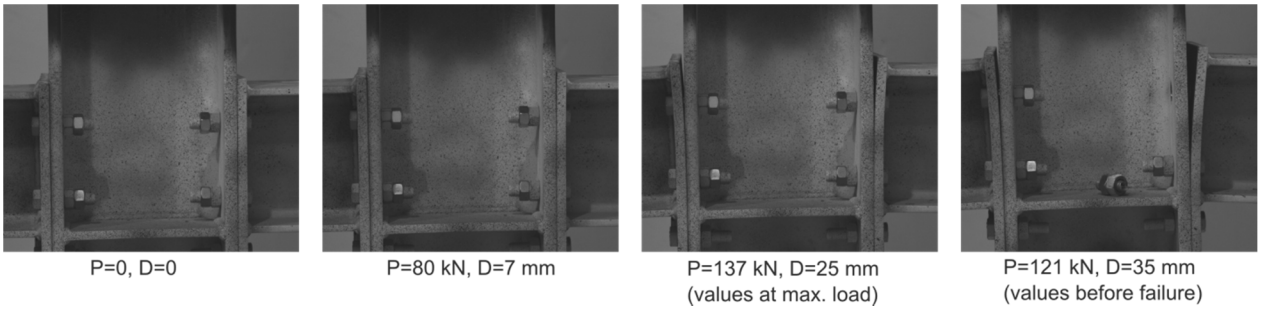

a) Test QS-RLD-3

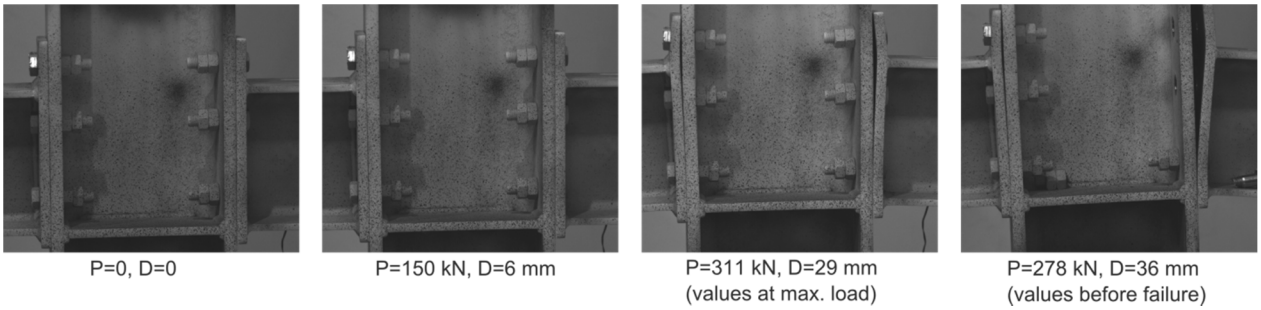

b) Test QS-DLD-4

Figure 8 - Deformation in tests QS-RLD-3 and QS-DLD-4 at four stages in the tests.

Post-print version of the paper by Grimsmo et al. in Int J Impact Eng, 85 (2015) 132-145
http://dx.doi.org/10.1016/j.ijimpeng.2015.07.001

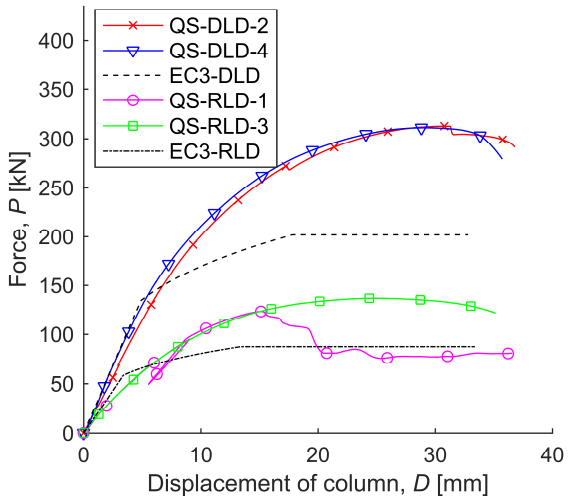

Figure 9 - Force-displacement curves from four quasi-static test and predictions with Eurocode 3 (EC3).

The force-displacement curves obtained from the four quasi-static tests are presented in Figure 9. Also included in this figure are the force-displacement curves predicted by the Eurocode 3 calculations, one for each load direction. Without further discussion, it is clear that the Eurocode 3 predictions are conservative in terms of resistance.

The experimental curves in Figure 9 are plotted until failure in the test specimens. As in Figure 8, fracture of two or more bolts was the failure mode in three of the tests, giving a sudden reduction of the force (not shown in Figure 9). Specimen QS-RLD-1 was however an exception. In this test, which was the first one in the experimental program, the force did not drop suddenly, but rather had a gradual decrease due to thread failure when D exceeded 15 mm. Thread failure should normally not happen in regular structural bolts, because the height of a nut is designed such that the intended fracture mode in bolt and nut assemblies is tensile failure of the bolt shank [16, 17]. With this argument in mind, two nuts were used in the remaining 11 tests to avoid thread stripping and thus improve the utilization of the capacity of the specimens. Photos of the two failure modes for bolts in tension are shown in Figure 10. From comparison of the force-displacement curves of tests QS-RLD-1 with QS-RLD-3 in Figure 9, it is obvious that both the maximum force and the corresponding displacement of the column are lower for the case of thread failure. Another particular feature associated with test QS-RLD-1 is that a sudden unloading can be observed at about 90 kN force and 8 mm displacement. This was due to unintended movement in the test rig. At further loading, the test curve continued fairly close to where it left off. The tests show

Post-print version of the paper by Grimsmo et al. in Int J Impact Eng, 85 (2015) 132-145
http://dx.doi.org/10.1016/j.ijimpeng.2015.07.001

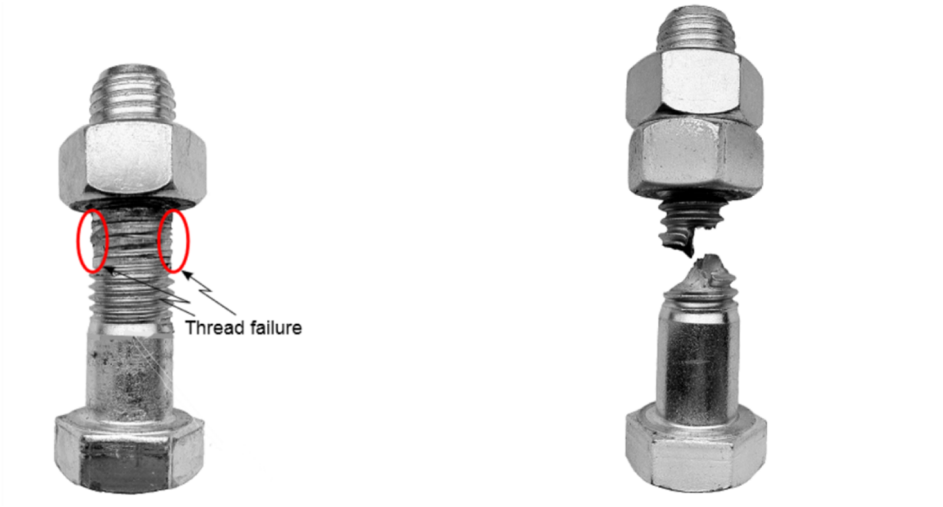

a) Thread failure (test QS-RLD-1)

b) Shank failure (all tests except QS-RLD-1)

Figure 10 - Photos of the two experienced bolt failure modes.

otherwise a decent repeatability, which indicates that the test set-up was adequate for the purpose of this study.

By comparing the force-displacement curves of tests QS-RLD-1 and QS-RLD-3 with QS-DLD-2 and QS-DLD-4 in Figure 9, it is obvious that the DLD configuration gave the highest initial stiffness and load capacity. This was expected because of the additional bolt row in the tension zone of the DLD configuration compared to the RLD configuration. On the other hand, there was a much smaller difference when comparing the ductility of the joints. Here, the ductility is interpreted as the maximum displacement of the column, which is related to the maximum rotational capacity of the joints. It is common to define the rotational deformation of joints as the change in angle between the member axes, see for instance Girão Coelho et al. [18]. However, since deformation of the joint configuration was slightly asymmetrical with respect to the centreline of the column, it was more convenient to use the displacement of the column as a measure of ductility rather than the rotation of the left and right joints.

3.2 Dynamic component tests

Figure 11 displays the deformation of the upper joint in two high-speed tests at four values of the displacement of the column. This displacement, D, was obtained from DIC analysis. The third picture frame shows the deformation when fracture was observed in one of the bolts. As in the quasi-static component tests, failure occurred by end-plate yield mechanisms and bolt fracture. The

Post-print version of the paper by Grimsmo et al. in Int J Impact Eng, 85 (2015) 132-145
http://dx.doi.org/10.1016/j.ijimpeng.2015.07.001

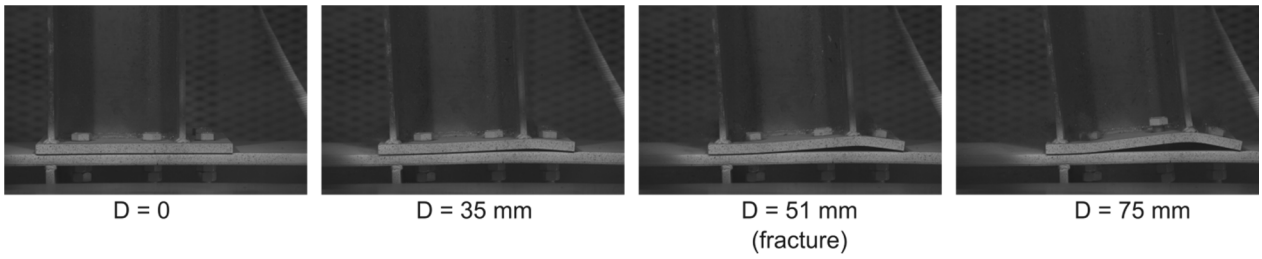

a) Test HS-DLD-11

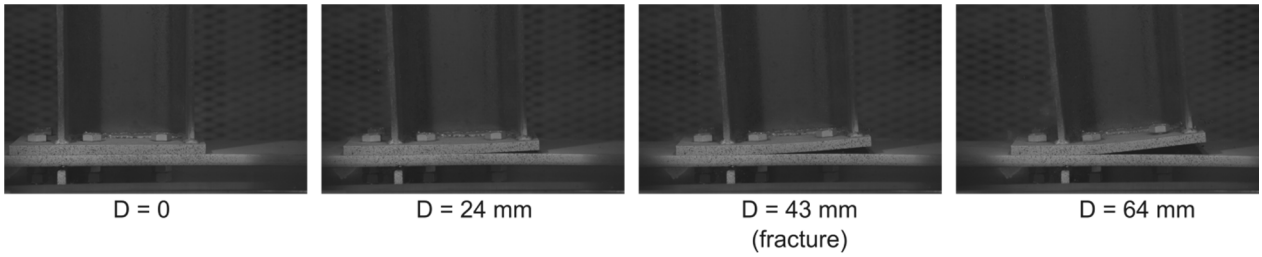

b) Test HS-RLD-12

Figure 11 - Deformation of the upper joint at four stages in tests HS-DLD-11 and HS-RLD-12.

typical duration of a test was between 5 and 10 ms. The elapsed time at fracture was determined by examining the camera recordings and observing when the head of one of the bolts had its first sudden movement in the direction normal to the end-plate. This indicated that some elastic energy had been released, which further implied fracture of the bolt. For the remainder of the discussion of the dynamic test results, the first visible movement of the column was chosen as the start of the test, and the onset of bolt fracture was defined as the end of the test. For the DLD tests, the bolts in the centre row fractured before the bolts in the row outside of the beam flange.

As experienced for the quasi-static tests, symmetry became eventually lost for the low-speed tests, and fracture took place at *one* joint. For the high-speed tests, however, fracture occurred at *both* joints nearly simultaneously and a more symmetric deformation pattern was achieved throughout the test, even after fracture. A possible explanation is that fracture occurred in a shorter time period for the high-speed tests and any asymmetrical forces acting on the column were not able to rotate the column noticeably within this time period.

Post-print version of the paper by Grimsmo et al. in Int J Impact Eng, 85 (2015) 132-145
http://dx.doi.org/10.1016/j.ijimpeng.2015.07.001

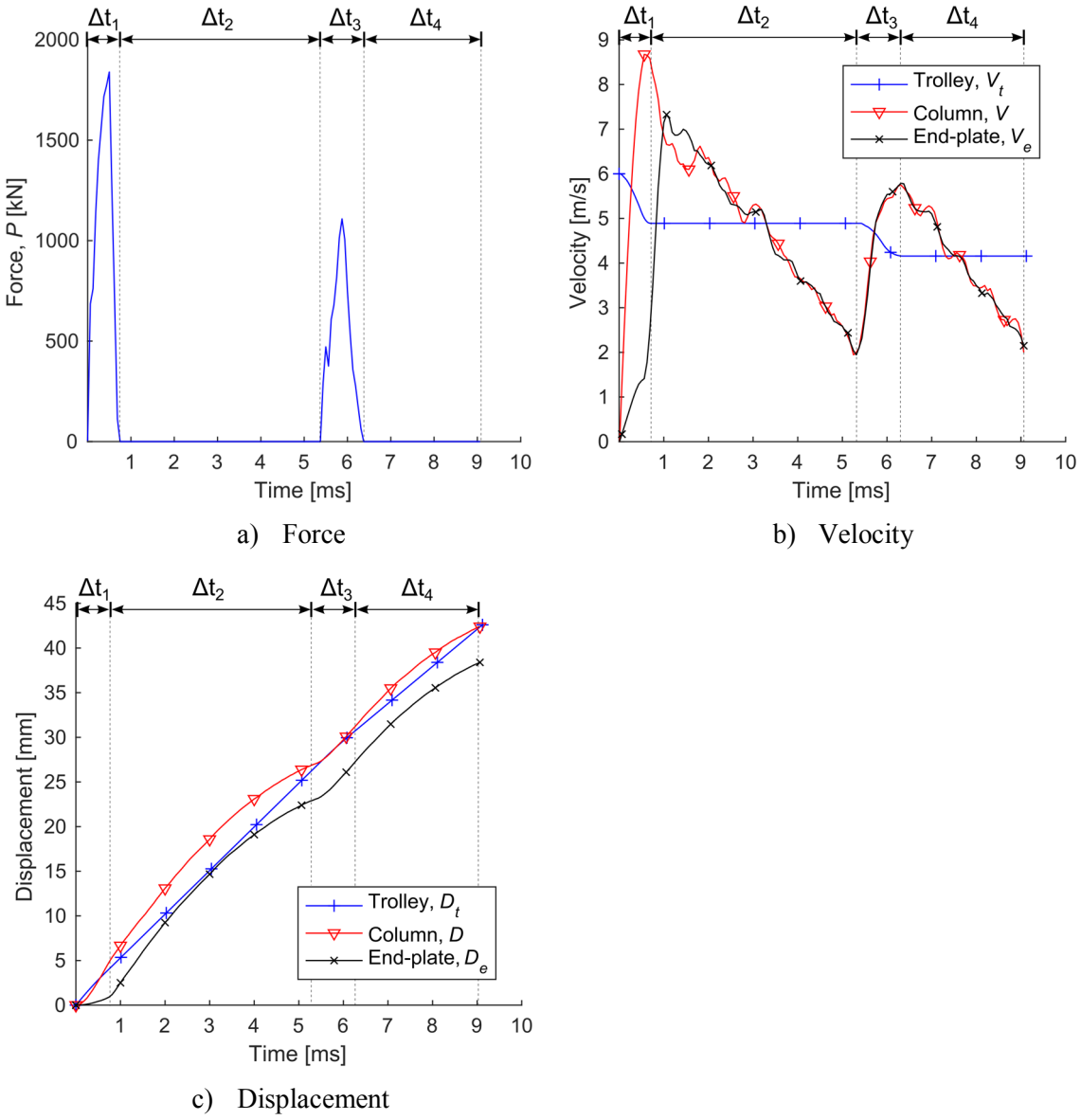

a) Force

b) Velocity

c) Displacement

Figure 12 - Results from test LS-RLD-8. Similar results were obtained from the other tests.

There was not continuous contact between the trolley and test specimen during a test, because the two bodies rather experienced a series of nearly elastic collisions. This will now be illustrated with the aid of Figure 12, which presents data acquired from test LS-RLD-8. The sub-figures a-c show respectively force vs. time, velocity vs. time, and displacement vs. time curves. The force P, velocity V_t, and displacement D_t of the trolley are all obtained from the load cell data of the trolley. Hanssen et al. [15] described how the displacement and velocity of the trolley can be calculated from the load cell signal. The velocity V and V_e, and displacement D and D_e, of respectively the

column and end-plate were found from DIC analysis of the joint region. The curves from the trolley and column in Figure 12 are considered first. During the period Δt_1, impact occurred between the trolley and column, as can be seen from the first peak in the force-time curve in Figure 12a. The column was consequently accelerated to a higher velocity than the initial velocity of the trolley during Δt_1, see Figure 12b, because the trolley had a significantly larger mass than the test specimen. Subsequently, the contact ceased between the trolley and test specimen at the end of Δt_1, and the force P became thus zero. The trolley, having a large inertia, obtained a constant velocity for a time period Δt_2, while the resisting forces of the joints decelerated the column. Observe from figure Figure 12c that the column displacement is larger than the trolley displacement, i.e. $D > D_t$, in the non-contact period Δt_2.

At the end of the period Δt_2, it is seen that the velocity of the column is less than of the trolley, i.e. $V < V_t$, which eventually led to $D \approx D_t$ again. Thus, a second impact took place during Δt_3, see the second peak in the force-time curve in Figure 12a. The effect from the second impact was again an acceleration of the column, which can be seen during Δt_3 in Figure 12b. The second peak in the force-time curve is lower, because the difference in velocities between the column and trolley was smaller. As has now been shown, LS-RLD-8 was subjected to two hits from the trolley before fracture. The number of hits for the other tests depended on the impact velocity of the trolley and the resistance of the specimen as defined by the load direction, i.e. RLD or DLD.

The response curves representing the end-plate behaviour in Figure 12b and c are now considered. Figure 12b displays how the movement of the end-plate was delayed, in the sense that it experienced no significant velocity before the end of the time period Δt_1. This led to a significant relative displacement of the column with respect to the end-plate, see Figure 12c. The relative displacement was up to 5 mm in some of the tests. Figure 13 depicts how an initial clearance of 2 mm between the bolt and bolt holes of the end-plate and column flange could facilitate a maximum of 4 mm relative displacement. The only resistance to such movement is the minor amount of friction introduced by the tightening moment of 80 Nm. Other contributors to the relative displacement were a minor rotation of the bolt and bearing deformation of the bolt holes, see Figure 13b, which was not observed in the quasi-static tests.

Post-print version of the paper by Grimsmo et al. in Int J Impact Eng, 85 (2015) 132-145
http://dx.doi.org/10.1016/j.ijimpeng.2015.07.001

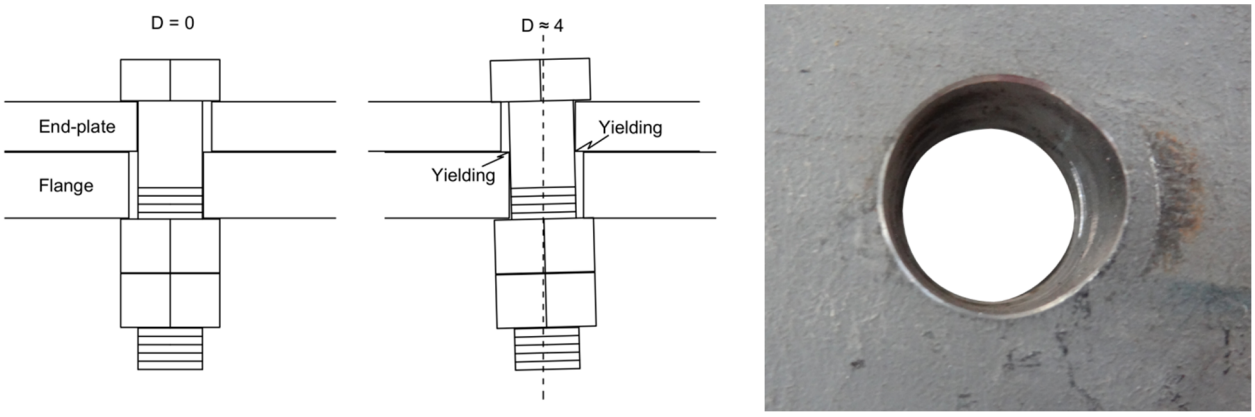

a) Relative displacement between the column flange and end-plate

b) Photo of a typical bolt hole in the column flange after a dynamic test.

Figure 13 - Local relative displacements and deformation around bolt holes.

Force-displacement curves for all the dynamic tests are given in Figure 14, where the pairs of replicate tests are plotted together. The displacement of the column *D* is used at the abscissa axes in the figure. In the first four dynamic tests, i.e. the low-speed tests in sub-figures a and b, the repeatability was not as good as for the last four tests with high speed, see sub-figures c and d. This was due to some changes made to the impact plate which was welded to the column, see Figure 6. The changes made were the following. After conducting tests LS-RLD-5 and LS-DLD-6 it was observed that there had been some local plastic deformation of the column web close to the point of impact. More specifically, a 1-2 mm shortening of the column was observed at the web, which occurred due to the imposed compression force. To avoid possible local buckling of the column web for the subsequent high-speed tests, a new impact plate was made for test LS-DLD-7. It was thicker and milled in such a way that the column web was not loaded, but rather the column flanges transferred the impact load. However, in this test the impact plate became plastically deformed. Thus, an improved impact plate was made and for the remaining tests, LS-RLD-8 to HS-RLD-12. This plate had higher yield strength than the previous ones, and a slightly different geometry such that it became stiffer (60 mm at its thickest section). Comparison of tests LS-RLD-5 and LS-RLD-8 in Figure 14a reflects this change in stiffness of the impact plate, because the first peak in force of LS-RLD-8 is higher, while it is shorter in terms of displacement.

Post-print version of the paper by Grimsmo et al. in Int J Impact Eng, 85 (2015) 132-145
http://dx.doi.org/10.1016/j.ijimpeng.2015.07.001

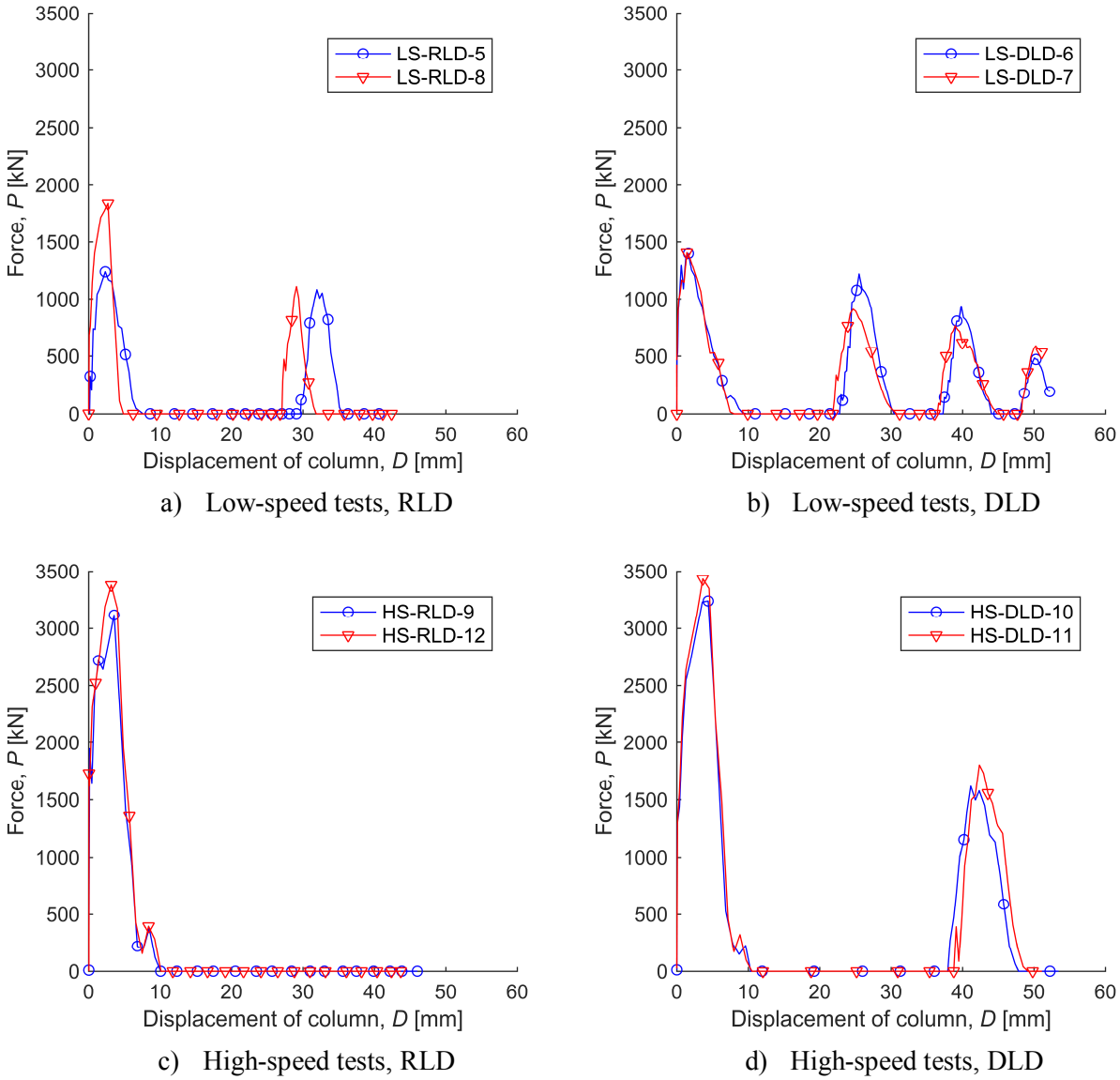

Figure 14 - Force- displacement curves for all eight dynamic tests. Each peak in force corresponds to a hit on the specimen by the trolley.

As opposed to the quasi-static tests, inertia was important for the dynamic tests, and the force levels were therefore enhanced. Note that the force level of the first peaks in Figure 14 is nearly the same for the two configurations RLD and DLD (disregard LS-RLD-8). This illustrates, as expected, that the inertia of the test specimen was independent of the orientation of the specimen. A difference in the results between the two configurations was the number of peaks before fracture. The DLD specimens had a higher force capacity and gave therefore more resistance to deformation, thus leading to a faster deceleration of the test specimen. This further led to more hits registered before

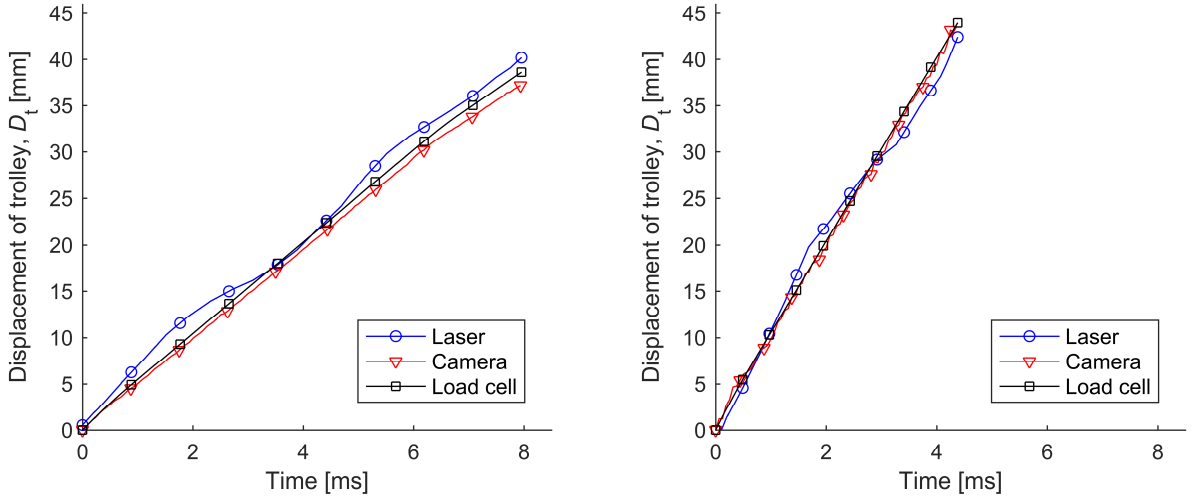

a) Test LS-RLD-5 b) Test HS-RLD-9

Figure 15 – Displacement of trolley in two representative dynamic tests as measured by laser, camera recordings, and integration of load cell data.

fracture for the DLD tests than for the RLD tests. Note also from Figure 14 that the force level was dependent on the impact velocity of the trolley; the force level was roughly around 1500 kN and 3300 kN for the low- and high-speed tests, respectively.

There were three available approaches to determine the displacement of the trolley, D_t, during the tests: camera recordings, laser measurements, and integration of load cell data. As a quality check, the displacements determined with the three measurement techniques were plotted together. Two tests are presented as examples in Figure 15. In general, there was a good agreement between the displacement measures, which gives confidence in the obtained load cell data. Note that the laser recordings in Figure 15 fluctuate slightly from the two other displacement measures. This is assumed to be due to vibration of the reflection plate under the trolley at which the laser pointed, see left-hand part of Figure 7.

3.3 Comparisons between quasi-static and dynamic component response

Figure 16 compares the force-displacement curves obtained from representative quasi-static and dynamic tests. As in the previous sections, the maximum displacements in these curves represent the displacement when fracture was observed in one or more bolts. The difference in force levels is obvious in Figure 16. Furthermore, there is also a significant dissimilarity in the displacement of the column at failure. As discussed previously, this displacement is a measure of the ductility of

Post-print version of the paper by Grimsmo et al. in Int J Impact Eng, 85 (2015) 132-145
http://dx.doi.org/10.1016/j.ijimpeng.2015.07.001

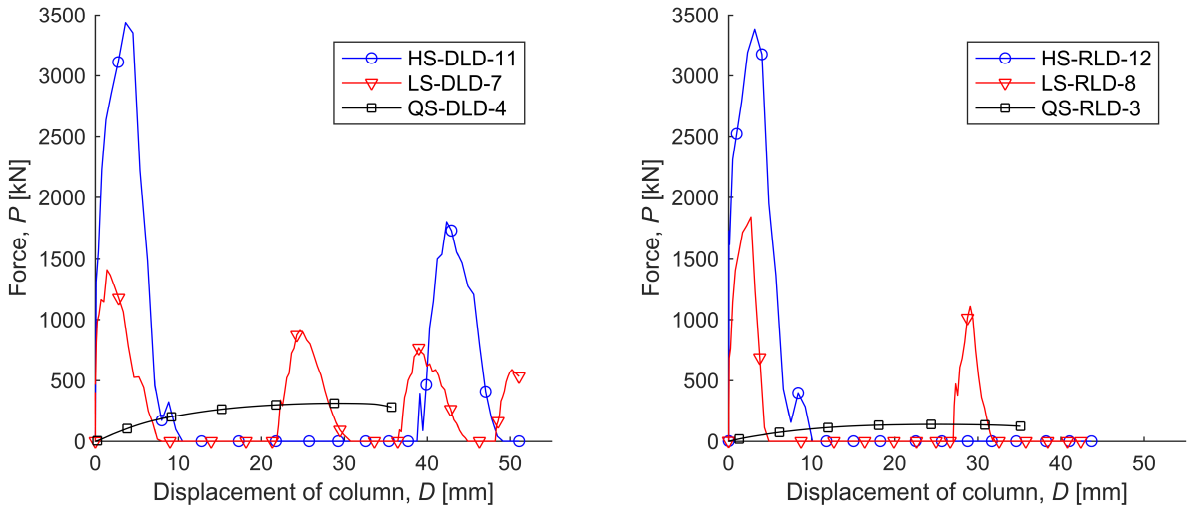

a) DLD tests b) RLD tests

Figure 16 - Comparison of force-displacement plots from quasi-static and dynamic tests.

the joints. From the differences in force levels and maximum displacements, it is obvious that the amount of external work, i.e. the force integrated over displacement, performed on the test specimens varied among the tests. This is studied in more detail in subsequent paragraphs.

For the quasi-static tests, integration of the load over the displacement gives readily the strain energy, or work, used to deform the test specimen. However, for the dynamic tests, the strain energy is more difficult to obtain, and a different approach is therefore needed. The energy put into the dynamic tests is the initial kinetic energy of the trolley, $K_{t,0}$. Assuming that the mechanical energy is conserved, the following energy balance can be set up:

$$K_{t,0} = K_t + K_s + U, \tag{1}$$

where K_t and K_s are the kinetic energies of the trolley and test specimen at the time of failure, respectively, and U is the strain energy associated with deformation of the test specimen. It is assumed that negligible amount of kinetic energy was transformed to stress waves, heat, and deformations at the boundaries. The energies $K_{t,0}$ and K_t were determined with relatively high certainty, while K_s was achieved by using the measured velocity V of the column and by assuming the velocity field shown in Figure 17. The beams are idealized as rigid bodies that rotate on the support points.

With the kinetic energies determined, it is possible to calculate the strain energy U from Equation (1). Figure 18a presents U as a function of the impact velocity of the trolley. It is clear

Post-print version of the paper by Grimsmo et al. in Int J Impact Eng, 85 (2015) 132-145
http://dx.doi.org/10.1016/j.ijimpeng.2015.07.001

from this figure that U increased as the impact velocity of the trolley was increased, and the DLD configuration absorbed most energy due to the higher moment resistance of the joints. A part of the reason for the significant increase in U is that the dynamic tests displayed a more symmetric deformation mode with respect to the centreline of the column, particularly for the high-speed tests. For example, two bolts at *each* of the joints fractured almost simultaneously in the high-speed RLD tests, whereas only two bolts fractured in the corresponding quasi-static and low speed tests. It is therefore obvious that more energy was required to deform the test specimens at high speed.

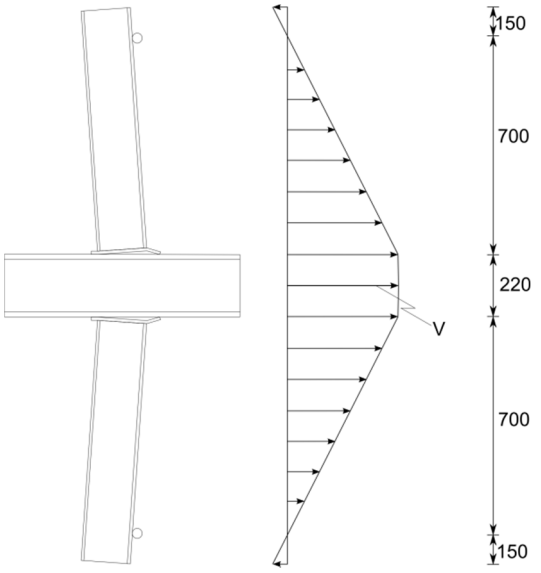

Figure 17 - Linear velocity field used to determine the kinetic energy of the test specimen at the time of fracture. V is the velocity of the column.

Post-print version of the paper by Grimsmo et al. in Int J Impact Eng, 85 (2015) 132-145
http://dx.doi.org/10.1016/j.ijimpeng.2015.07.001

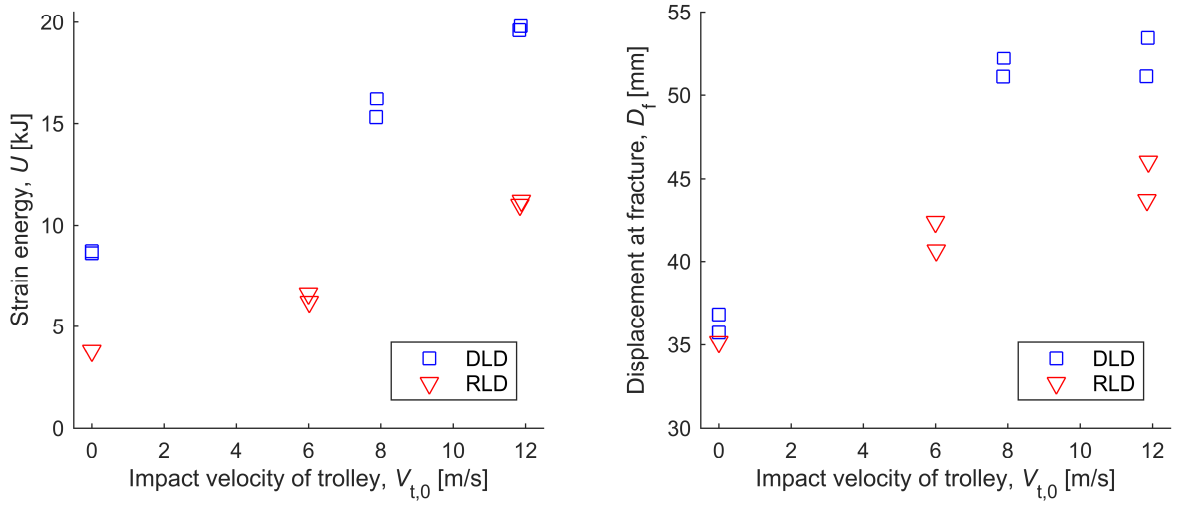

a) Strain energy U used to deform test specimen

b) Displacement at fracture, D_f

Figure 18 - Strain energy absorption and displacement at fracture for different impact velocities of the trolley.

Another contribution to the increase in strain energy U is likely caused by the strain-rate sensitivity of the steel material, see Figure 3a, because higher test speeds induced larger strain rates. The strain rate in the bolts was estimated from the camera recordings; the development of opening between the end-plates and column flanges at the position of the fracturing bolts was determined with DIC analysis. This opening indicates the tensile deformation the bolts have experienced. Thus, estimates of the strain rate in the bolts can be found from the relation $\dot{\varepsilon}_b \approx v/L_0$, where v is the average opening rate obtained from DIC analysis and L_0 is the initial length of the part of the bolt that was deformed. Most of the tensile deformation occurred in the threaded part of the bolt due to the smaller cross-sectional area there, see Figure 19. The value of L_0 was therefore set to 8 mm. Tests HS-DLD-11 and HS-RLD-12, for example, gave strain-rates of approximately 110 and 130 s^{-1}, respectively. It is therefore reasonable to assume that higher stresses, due to the increased strain-rate in the dynamic tests, led to increased energy absorption in the plastic deformation processes. Furthermore, it is expected that some energy was absorbed in axial compression of the column in the dynamic tests. Two other contributors to the differences in U are connected to Figure 13b and Figure 19, as significant bolt hole elongation and shear deformation of the bolts only occurred for the dynamic tests.

Post-print version of the paper by Grimsmo et al. in Int J Impact Eng, 85 (2015) 132-145
http://dx.doi.org/10.1016/j.ijimpeng.2015.07.001

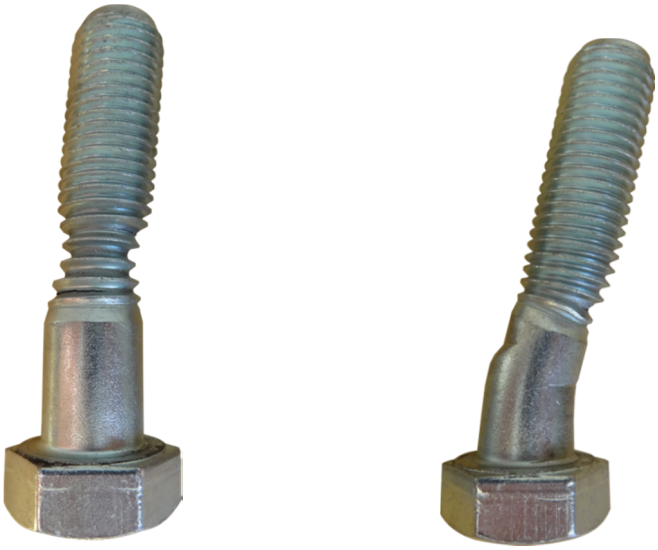

a) Quasi-static b) Dynamic

Figure 19 - Deformed bolts originating from quasi-static and dynamic (high-speed) tests.

Figure 19 gives two examples of deformed but not fractured bolts, one from a quasi-static test and one from a dynamic test. The main difference is the shear deformation observed in the unthreaded part of the bolt from the dynamic test. The relative movement between the end-plate and the column flange in the dynamic tests (see Figure 12c) seems to have caused shear deformation and more pronounced bending of the bolt. Such deformations were not visible in any of the bolts from the quasi-static tests. Note that not all the bolts from the dynamic tests exhibited the same amount of shear deformation, as it depended on the location of the bolt in the joint and the impact velocity.

As seen in Figure 18b, the displacement of the column at fracture, D_f, became larger as the impact velocity of the trolley increased. As opposed to in the dynamic tests, there was virtually no relative displacement between the end-plate and column flange in the quasi-static tests, which explains some of the increase in D_f when comparing the quasi-static and dynamic tests. Another part of the increase in D_f can be explained by the elongation of the bolt holes discussed in Section 3.2. A more important factor, however, is likely linked with the fact that the slight rotation of the column was less noticeable as the impact velocity increased. This slight rotation allowed the bolts at one joint to fracture at a smaller displacement of the column compared to a case with no rotation.

Post-print version of the paper by Grimsmo et al. in Int J Impact Eng, 85 (2015) 132-145
http://dx.doi.org/10.1016/j.ijimpeng.2015.07.001

4 Discussion

Menkes and Opat [19] demonstrated that doubly-clamped aluminium beams experienced shear failure at the supports before the development of a flexural mode of response when subjected to high-intensity short-duration transverse pressure loading. Analogously, the joints in the current study became subjected to larger shear forces in the dynamic tests than in the quasi-static tests, and the bolts consequently experienced more shear deformation, as seen in Figure 19. From these observations it seems that shear failure of the joints is possible in impact load conditions. It is therefore important to bear in mind that, according to Eurocode 3 predictions, insufficient shear resistance was far from being the determining failure mechanism.

It is obvious that bolt failure in shear would be even more likely in the dynamic tests if the beams had more inertia, as would be the case in the presence of for instance attached floors with large mass. In addition to increasing the inertia of the beams, possibly attached floor slabs and secondary beams would affects the stiffness, moment and rotational capacities of the joints. As an example, Yang and Tan [7] showed that joints with attached composite steel-concrete slabs had higher static load-carrying capacities than bare steel joints when subjected to column-loss load conditions.

Shear failure in joints is generally unfavourable since it is a more brittle failure mode, where the joints experience less deformation prior to failure. This argument also applies for severe impulsive loading, because shear failure most likely leads to less energy absorbed by the joints.

The joint configuration at hand became more ductile when subjected to impact loading, in the sense that the displacement at fracture, D_f, increased as the test speed increased. On the contrary, Tyas et al. [4] showed that joints with flexible end-plate connections became less ductile in a dynamic test compared to in a quasi-static test. It is thus clear that more research should be carried out to improve the understanding on this topic.

As already mentioned, two nuts were used throughout all tests except for test QS-RLD-1 to avoid thread stripping. Therefore, a problem that was not addressed in the present investigation was whether thread stripping was most likely to occur at quasi-static or dynamic conditions. Mouritz [20] performed impact tests on bolts of mild steel in tension and found that the failure load decreased at increased strain rate. However, the failure mechanism apparently did not change.

Fransplass et al. [21, 22] showed that the failure mode in threaded steel rods did not only depend on the strain rate, but also the thread engagement and grip length.

5 Summary and conclusions

A double-sided beam-to-column joint configuration has been tested at quasi-static and dynamic loading conditions. Four tests were conducted under quasi-static loading using a hydraulic actuator, while eight dynamic tests were carried out in a pendulum accelerator test rig designed for impact testing. Six of the specimens were loaded such that the bending moment acted in the direction the joints were designed for, and the other six specimens were loaded in the reverse direction. In the dynamic tests, the test specimens were impacted by a trolley of 727 kg at impact speeds that ranged between 6 and 12 m/s. The tests provide an experimental data base that can be used for validation of numerical simulations.

The test specimens had joints with bolted end-plate connections, which were designed such that failure by end-plate yield-mechanisms and bolt fracture gave the lowest resistance according to Eurocode 3. This was also observed as the failure mode for both for the quasi-static and dynamic tests. However, it was argued that shear failure of the bolts seemed more likely in impact load scenarios, in particular if the parts of the structure adjacent to the joints have large inertia. More research is needed before it can be determined whether the resistance formulas of Eurocode 3 can be used to predict failure modes in steel joints subjected to extreme impulsive loads.

The tests showed that more energy was required to obtain fracture in the joint configuration when impact velocities increased. The increased absorption of strain energy in the dynamic tests is associated with a more symmetrical deformation mode, enhanced strain-rate hardening, and larger local deformations of parts of the joints. Also, the displacement of the column at fracture increased with higher impact velocities, which can be interpreted as an increase in the ductility of the joints for higher loading rates. From these observations, it can be concluded that the investigated joint behaved in a preferable manner. However, knowledge of the dynamic behaviour of bolted steel joints in general is still relatively limited, and more tests and numerical simulations are therefore in order.

Acknowledgements

The work has received economical support from the Research Council of Norway through the SFI scheme. The authors would like to express their gratitude to Mr T. Auestad and Mr T. Wisth for their assistance with the experimental work. Acknowledgements are also given to Prof. emeritus P. K. Larsen for general feedback on the work.

References

[1] A.S. Daryan, M. Ziaei, S.A. Sadrnejad, The behavior of top and seat bolted angle connections under blast loading, J Constr Steel Res, 67 (2011) 1463-1474.
[2] C. Liu, K.H. Tan, T.C. Fung, Dynamic behaviour of web cleat connections subjected to sudden column removal scenario, J Constr Steel Res, 86 (2013) 92-106.
[3] T. Sabuwala, D. Linzell, T. Krauthammer, Finite element analysis of steel beam to column connections subjected to blast loads, Int J Impact Eng, 31 (2005) 861-876.
[4] A. Tyas, J.A. Warren, E.P. Stoddart, J.B. Davison, S.J. Tait, Y. Huang, A Methodology for Combined Rotation-Extension Testing of Simple Steel Beam to Column Joints at High Rates of Loading, Exp Mech, 52 (2012) 1097-1109.
[5] B. Yang, K.H. Tan, Experimental tests of different types of bolted steel beam-column joints under a central-column-removal scenario, Eng Struct, 54 (2013) 112-130.
[6] Department of Defence (DOD), Structures to resist the effects of accidental explosions: Unified Facilities Criteria (UFC 3-340-02), US Department of Defence, Alexandria, VA, 2008.
[7] B. Yang, K.H. Tan, Behavior of composite beam-column joints in a middle-column-removal scenario: Experimental tests, J Struct Eng (United States), 140 (2014).
[8] H.S. Lew, J.A. Main, S.D. Robert, F. Sadek, V.P. Chiarito, Performance of steel moment connections under a column removal scenario. I: Experiments, J of Struct Eng (United States), 139 (2013) 98-107.
[9] J.E. Karns, D.L. Houghton, J.-K. Hong, J. Kim, Behavior of Varied Steel Frame Connection Types Subjected to Air Blast, Debris Impact, and/or Post-Blast Progressive Collapse Load Conditions, in: Structures Congress 2009, pp. 1-10.
[10] E.P. Stoddart, M.P. Byfield, J.B. Davison, A. Tyas, Strain rate dependent component based connection modelling for use in non-linear dynamic progressive collapse analysis, Eng Struct, 55 (2013) 35-43.
[11] R. Rahbari, A. Tyas, J. Buick Davison, E.P. Stoddart, Web shear failure of angle-cleat connections loaded at high rates, J Constr Steel Res, 103 (2014) 37-48.
[12] European Committee for Standardization (CEN), NS-EN 1993-1-8:2005, Eurocode 3: Design of steel structures - Part 1-8: Design of joints, Norwegian Standard, 2009.
[13] V. Vilamosa, A.H. Clausen, E. Fagerholt, O.S. Hopperstad, T. Børvik, Local measurement of stress-strain behaviour of ductile materials at elevated temperatures in a split-Hopkinson tension bar system, Strain, 50 (2014) 223-235.

[14] S. Dey, T. Børvik, O.S. Hopperstad, M. Langseth, On the influence of constitutive relation in projectile impact of steel plates, Int J Impact Eng, 34 (2007) 464-486.
[15] A.G. Hanssen, T. Auestad, T. Tryland, M. Langseth, The kicking machine: A device for impact testing of structural components, Int J Crashworthiness, 8 (2003) 385-392.
[16] International Organization for Standardization (ISO), ISO 898-2, Mechanical properties of fasteners made of carbon steel and alloy steel - Part 2: Nuts with specified property classes - Coarse and fine pitch thread, ISO, Switzerland, 2012.
[17] J.A. Swanson, Characterization of the strength, stiffness and ductility behavior of T-stub connections, in, Georgia Institute of Technology, Atlanta, GA, 1999.
[18] A.M. Girão Coelho, F.S.K. Bijlaard, L. Simões da Silva, Experimental assessment of the ductility of extended end plate connections, Eng Struct, 26 (2004) 1185-1206.
[19] S.B. Menkes, H.J. Opat, Broken beams - Tearing and shear failures in explosively loaded clamped beams, Exp Mech, 13 (1973) 480-486.
[20] A.P. Mouritz, Failure mechanisms of mild steel bolts under different tensile loading rates, Int J Impact Eng, 15 (1994) 311-324.
[21] H. Fransplass, M. Langseth, O.S. Hopperstad, Tensile behaviour of threaded steel fasteners at elevated rates of strain, Int J Mech Sci, 53 (2011) 946-957.
[22] H. Fransplass, M. Langseth, O.S. Hopperstad, Numerical study of the tensile behaviour of threaded steel fasteners at elevated rates of strain, Int J Impact Eng, 54 (2013) 19-30.

Appendix

Some dimensions of the trolley and the load cell located at the front of the trolley are given in Figure 20. As can be observed from the figure, the largest component of the trolley is the plate with the dimensions 1350 mm x 730 mm and a thickness of 50 mm. The cylindrical nose of the trolley, seen at the far right in Figure 20, has a diameter of 80 mm and length of a 100 mm. The nose was welded to a 20 mm thick plate, which was bolted to the load cell. Further, the other end of the load cell was connected to a plate with 50 mm thickness that was bolted to the trolley. The load cell itself, shown in the lower part of Figure 20, was instrumented with strain gauges in the section with smallest cross section area, i.e. the section having external radius 60 mm and internal radius 40 mm.

Post-print version of the paper by Grimsmo et al. in Int J Impact Eng, 85 (2015) 132-145
http://dx.doi.org/10.1016/j.ijimpeng.2015.07.001

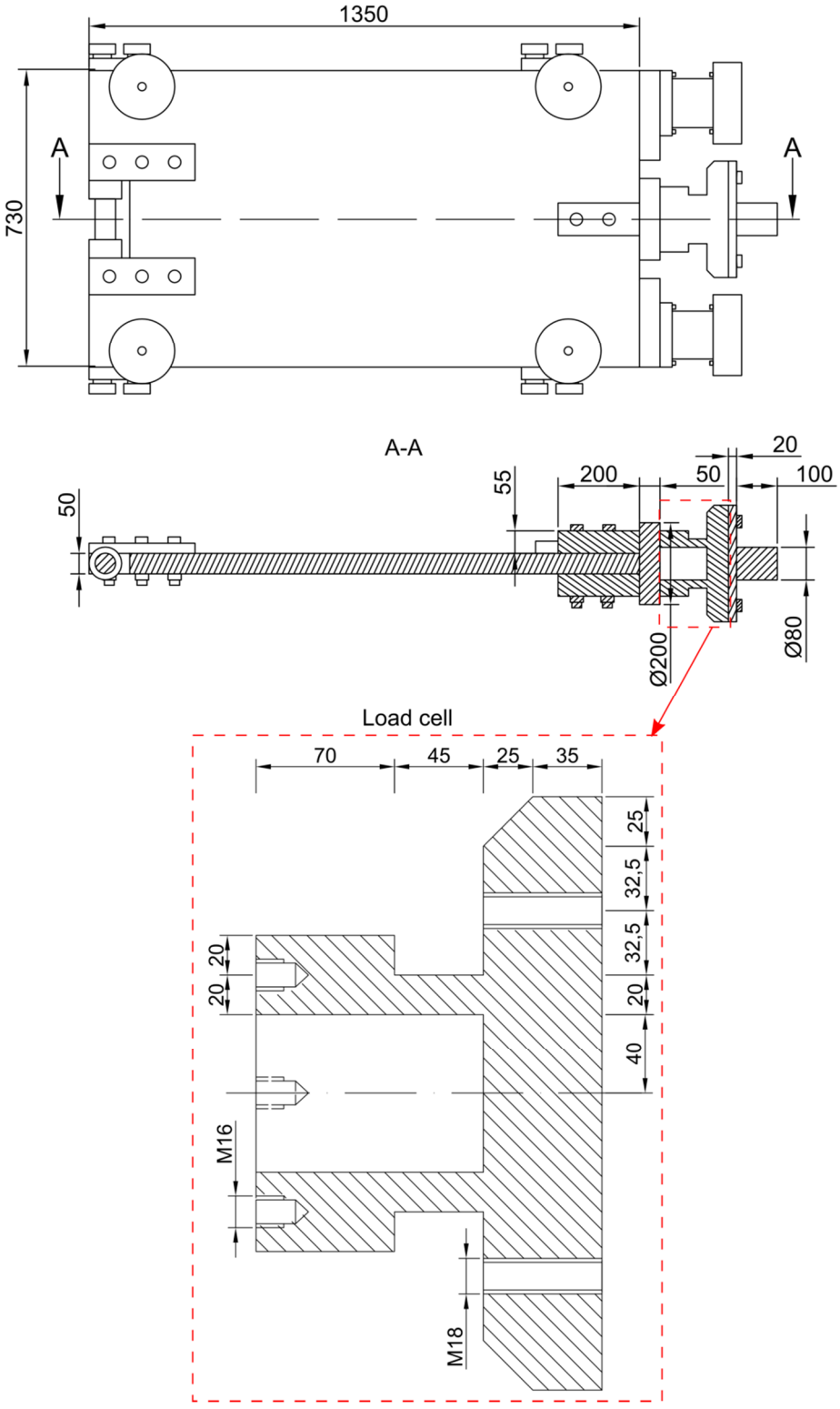

Figure 20 - Dimensions of the trolley and the load cell.